ASIA-PACIFIC SOLAR RESEARCH CONFERENCE

PEER REVIEWED
ASIA-PACIFIC
SOLAR RESEARCH CONFERENCE

Paing

Modelling and experimental validation of natural convection heat loss from a solar hot water storage tank

Si Thu Paing[1], Timothy Anderson[1] and Roy Nates[1]

[1]*Department of Mechanical Engineering, Auckland University of Technology, Auckland, New Zealand*

Email: timothy.anderson@aut.ac.nz

Abstract

Solar hot water storage tanks are required to store thermal energy collected during the day due to the intermittent nature of the resource. However, the performance of these storage devices is characterised by heat losses to the surroundings. Previous studies have discussed the effect of a tank's aspect ratio, wall thickness and the inner lining material on its thermal performance. However, the role that natural convection plays in the heat loss from these tanks has not been particularly well discussed.

In this study, CFD was used to investigate the transient cooling of a 200 L storage tank (1.22m tall) with a view to understanding the natural convection inside the tank induced by sidewall heat losses. The computational methodology was validated with experimental temperature measurements and particle image velocimetry (PIV) data. PIV data was obtained for the top (860 to 1220 mm of tank height), middle (440 to 790 mm of tank height) and bottom (35 to 310 mm) of the tank with different boundary layer thicknesses and peak velocities observed in the three sections.

It was found that at the top and bottom of the tank the velocities were low, in the order of 1-3 mm/s, while in the middle section velocities were approximately 3-7 mm/s. Interestingly it was also found that in addition to the variation in the velocity, there was a thickening of the boundary layer in the middle tank section, while and the top and bottom it remained notably thinner. From this, it could be suggested that the low velocity and thin boundary layer at the top is due to the initial formation of the velocity boundary layer. The fluid velocity then increases along with the growth of the boundary layer as the fluid near the wall flows downward due to the sidewall heat loss. However, near the bottom of the tank, the fluid detaches from the wall and mixes with surrounding fluid of same density resulting in the thinning boundary layer. The observed variations of boundary layer thickness and velocity inside the boundary layer along the height of the tank could be useful in elucidating measures to reduce heat loss to the surroundings and improve thermal performance of solar thermal hot water storage tanks.

1. Introduction

The heat loss from solar thermal storage tanks can play a significant role in determining their overall performance. In their review of work on thermal storage tanks, Candra and Matsuka (2019) concluded that geometric factors such as the aspect ratio, wall thickness, shape played an important role in the heat loss encountered by a tank. Similarly, they noted that the materials used in a tank play a key role in static heat losses but for dynamic operations, the inlet mixing was the key determinant of heat loss. However, as many storage tanks experience

extended periods of 'static' operation, Fan and Furbo (2012) investigated the natural convection inside a tank due to standby heat losses. The authors observed that the volumetric flow rate of the convective currents in their tank reduced significantly, from 6 L/min to 0.12 L/min, with an increase in aspect ratio from 1 to 5. They attributed this reduction to the increased thermal stratification inside the tank at higher aspect ratios. Also exploring issues of tank geometry, Yang et al. (2016) found that tanks with lower surface area to volume ratio possess high thermal storage capacity. However, tanks with sharp corners showed the maximum stratification while those with flat horizontal surfaces indicated the lowest and an intermediate degree of stratification is observed in the ones with hemispherical walls.

Given the obvious role materials play in the determination of heat loss from a storage tank, Armstrong et al. (2014) studied the impact of the wall thickness of a tank on its performance. They reported that decreasing the wall thickness of a stainless-steel tank from 1 mm to 0.7 mm resulted in a loss of useable hot water volume of 13%. Several other studies have also found that the material used in a tank influences heat loss due to conduction vertically along the tank wall, which leads to strong natural convection inside the tank (Jularia and Gupta, 1982; Miller, 1977; Nelson et al, 1999). This can be mitigated by either choosing the tank material that has similar thermal conductivity to that of a fluid to be stored or insulating the inner side of the tank with a suitable lining material (Gasque et al, 2015; Shyu and Hseih, 1987).

As Fan and Furbo (2012) found, heat loss during static operation of a hot water tank leads to natural convection inside the tank, which is governed by a coupled thermal and hydrodynamic phenomenon. From this, it is reasonable to assume that if the temperature distribution in a numerical tank model is well-validated, it is also capable of estimating the flow patterns, although they are not directly validated (Oliveski 2000). However, it is desirable to validate both temperature and velocity profiles if possible, to truly understand the heat loss from thermal storage tanks. One way of achieving this would be with flow visualization, however studies that employ flow visualization techniques to investigate natural convection inside storage water tanks are relatively scarce. A few studies on vertical mantle hot water tanks have been conducted by Shah et al. (1999) and Knudsen et al. (2005). The former studied the flow structure in the mantle and observed flow recirculation driven by buoyancy, while the latter found that stratification can be maintained in the inner tank located above the mantle even when the hot water temperature at the mantle inlet is lower than the existing water temperature in the tank.

Given the relative paucity of studies on both the thermal and hydrodynamic behaviour of natural convection in thermal storage tanks, this work aimed to explore both aspects, with a view to determining how heat loss from these tanks could be reduced.

2. Experimental Setup

In order to deliver an understanding of both the thermal and hydrodynamic behaviour of the natural convection in a storage tank, an experimental tank was developed. The experimental tank was constructed as a square cylinder 400 mm x 400 mm with a height of 1220 mm, resulting in a capacity of approximately 200 litres. In order to study the hydrodynamic behaviour of the natural convection in the tank, due to heat loss, it was necessary to allow the optical access, hence the tank was fabricated from 15 mm thick acrylic sheet.

To examine the thermal behaviour, the tank was initially filled with well mixed water heated to 40 ˚C. The temperature of the water at various heights within the tank was measured by eight type-T thermocouples with an accuracy of ±1 ˚C, while a ninth sensor was used to monitor the surrounding air temperature. A data acquisition system (Picolog TC-08) was used to record

the temperatures at ten-minute intervals as the tank lost heat to the surrounding air. A schematic of the experimental setup is shown in Figure 1.

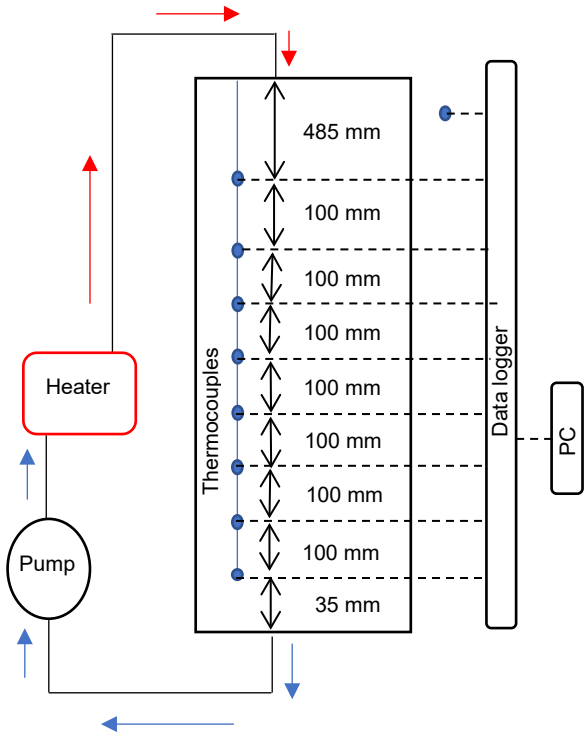

Figure 1. Experimental setup for temperature measurement

To capture the hydrodynamic flow in the tank as it lost heat to the surroundings, particle image velocimetry (PIV) was performed using a MicroVec PIV system. This system includes a dual-pulse PIV laser and a CCD camera that are synchronized with the help of a synchronizer (MicroPulse725), as shown in Figure 2. The laser beam is generated by a 2000 mW DPSS laser of 532 nm wavelength and is transformed into a laser sheet by optics to illuminate the tracer particles. A CCD camera with a frame rate of 16 fps and a resolution of 2456 x 2048 pixels is used to record the flow patterns. PIV measurements were performed over a 112.5-second period at a frequency of 4Hz (4 double exposures per second), hence obtaining 450 pairs of images captured at a 40 ms interval, which is in synchronization with the laser pulse delay. The captured image pairs were averaged and processed in the PIVLab software package, using a cross-correlation algorithm with an interrogation window size of 32x32 pixels

and a 50% overlap (i.e. the distance between two centres of adjacent interrogation areas is 16 pixels in each direction) to improve the resolution of the vector map.

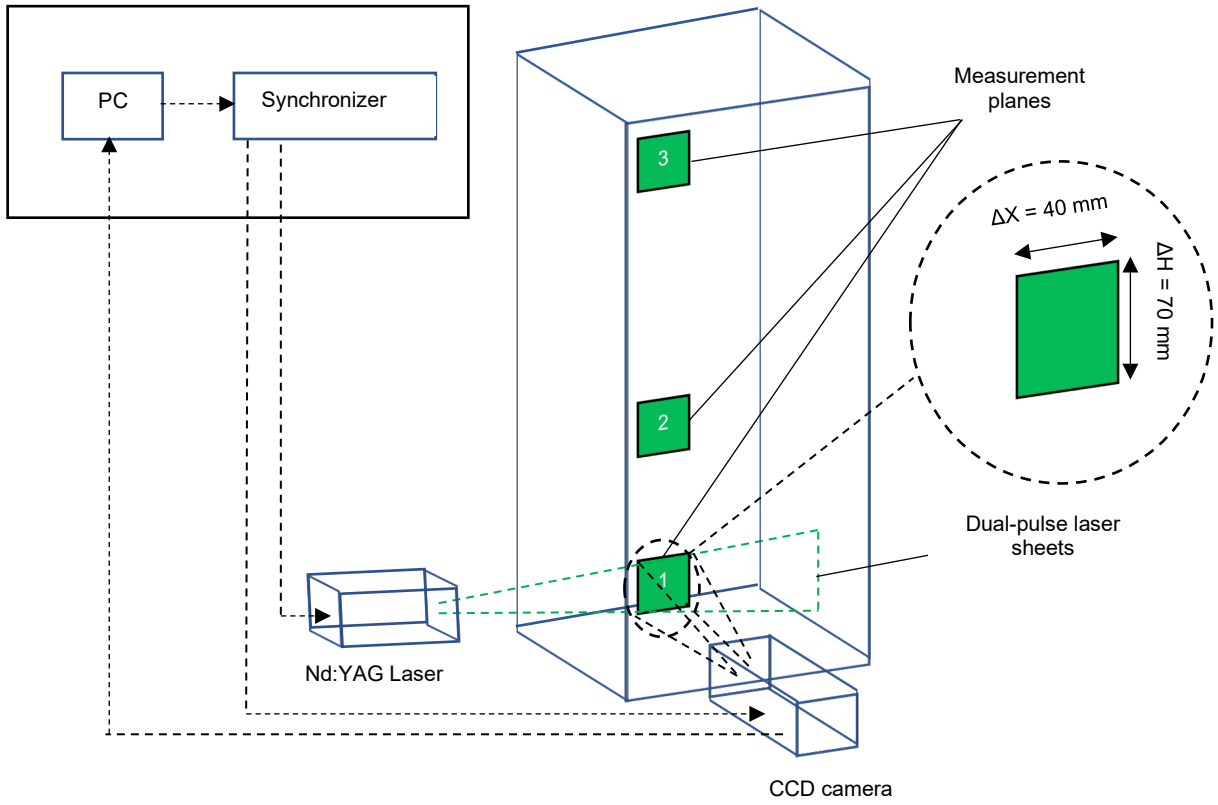

Figure 2. Experiment setup for PIV measurement

In seeding the flow with particles, a mixture of 20 and 50 μm round-shaped polyamide particles (Dantec Dynamics) with a density of 1030 kg/m^3 were added to the water. PIV images were taken along the wall, as the tank cooled, while the water temperatures were simultaneously recorded. The details of measurement planes at which PIV images were taken are shown in Table 1.

Table 1. Locations of measurement planes with respective recorded time measured from the beginning of the experiment

Measurement plane	Width, X (mm)	Height, H (mm)	Elapsed time (min)
1	0-40	40-110	10
2	0-40	315-385	30
3	0-40	1150-1220	80

3. Numerical model

To further understand the flow behaviour in the tank, a computational fluid dynamics (CFD) analysis was undertaken to predict the flow field in the tank when subject to standing heat loss. A numerical model of the tank was developed using the CFD code, ANSYS Fluent 18.2. A two-block structured mesh consisting of a fluid domain (water) and a solid domain (tank walls) was used to model the tank. To obtain better resolution of the flow and heat transfer near the tank wall, a boundary layer mesh with 20 layers was created, with a first-row thickness of 0.1 mm and a growth factor of 1.2. A mesh independence study was performed with three meshes having cell sizes in the range of 4-15 mm.

To ensure that the solution was independent of the time step size, solution time intervals in the order of 1-2 s were used, as suggested in the literature (Yang et a. 2016). A grid convergence index (GCI) with a safety factor of 1.25 was applied for the grid independence analysis, as suggested by Roache (1998). The calculated GCI between the coarsest and finest mesh with respect to average temperature of the tank showed a maximum error of 0.007%, indicating that a mesh with 935,424 cell elements with an average cell sizing of 10.11 mm, as shown in Figure 3 (a-c), was satisfactory. Similarly, a time step of 2 s was found to be adequate for this study. Based on the Rayleigh number obtained, and in line with studies on natural convection flow on a vertical flat plate (Vliet and Liu, 1969; Kang and Chung, 2010), it was hypothesized that the flow regime was laminar and modelled as such. For comparison with both temperature and PIV, the tank model was segmented into eight sections (S1-S8) since spatial variations in temperature across the width are negligible in comparison to those along the height (Oliveski, 2000). Therefore, each thermocouple reading from the experiment corresponds to the average temperature of the corresponding section as shown in Figure 3 (d).

Now, in order to accurately represent the boundary heat loss experimental temperature data was fitted based on Newton's law of cooling to obtain the overall heat transfer coefficient of each section over the duration of the simulation, as suggested by Mawire and Taole (2013).

As such, the rate of change of temperature of a section can be estimated by an exponential decay given by Equation 1.

$$\frac{\partial T_s}{\partial t} = -a(T_i - T_a)e^{-at} \tag{1}$$

The rate of heat loss from the tank can be written as Equation 2.

$$\rho_s c_{p,s} A_T h_s \frac{\partial T_s}{\partial t} = U_s A_s (T_s - T_a) \tag{2}$$

where T_s is the average temperature in a section, a is a constant, $(T_i - T_a)$ is the initial temperature difference between the average temperature of a section and the ambient temperature, $c_{p,s}$ is the specific heat capacity in a section, A_T is the cross sectional area of the tank, h_s is the height of a section, U_s is the overall heat transfer coefficient of a section, A_s is the surface area of a section.

Hence, the overall heat transfer coefficient of a section, U_s can be expressed as shown in Equation 3.

$$U_s = \frac{1}{\frac{1}{h_{int}} + \frac{L}{k_{wall}} + \frac{1}{h_{ext}}} \tag{3}$$

where h_{int} is the internal convective heat transfer coefficient, L is the tank wall thickness, k_{wall} is the thermal conductivity of the tank wall, h_{ext} is the external convective heat transfer coefficient.

In addition, convective boundary conditions were imposed on the outer walls as well as the top and bottom ends to simulate static operation.

At the top and bottom walls, this was given by Equation 4

$$-k_{wall}\frac{\partial T_{wall}}{\partial H} = h_{ext}(T_{wall} - T_a) \quad (4)$$

And at the side wall, by Equation 5, where T_{wall} is the tank wall temperature.

$$-k_{wall}\frac{\partial T_{wall}}{\partial X} = h_{ext}(T_{wall} - T_a) \quad (5)$$

Since the external heat transfer coefficient for each section needs to be specified in the CFD model, they were calculated using Equation (3) with known internal convective heat transfer coefficients and fixed heat conduction resistance by ensuring that the computed overall heat transfer coefficients are the same as those in the experiment, over the sampling period of 24 hours. The obtained external heat transfer coefficients along with measured ambient temperatures were specified by means of User Defined Function.

To account for buoyancy, the Boussinesq approximation was used in this study; this assumes that the thermophysical properties of water are constant except the density in the buoyancy term given in the momentum equation. Finally, the initial temperature of the water in the CFD model was 40˚C as with the experiment.

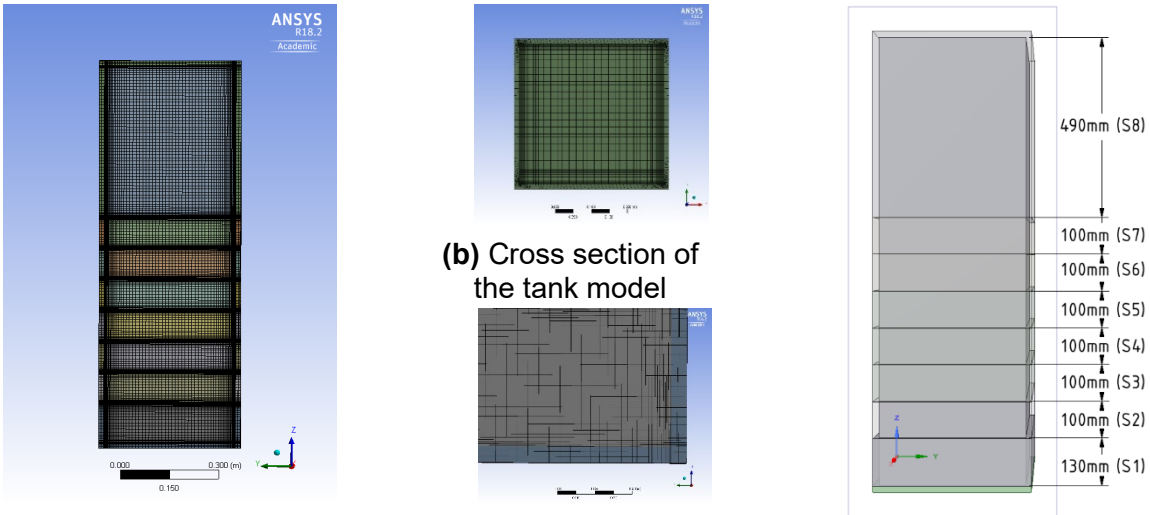

(a) Vertical cut plane of the tank model

(b) Cross section of the tank model

(c) An enlarged view of the corner

(d) Tank sections (S1-S8)

Figure 3. Mesh employed in the CFD model

4. Results and Discussion

4.1. Temperature profile

As a baseline, the thermal behavior of the storage tank was characterized using a transient cooling test. This static cooling test was conducted on the experimental tank with an initial uniform temperature of 40˚C and an average surrounding air temperature of 24.5˚C, with the same conditions modelled in the CFD solver. Figure 4 shows the measured, and CFD predicted, temperatures in the tank over a 24-hour period.

The temperatures show that after 10 minutes there has been a gradual decrease in temperature from 40˚C to 39.2˚C at the bottom of the tank. As the tank continues to cool down, the water temperature at the bottom decreases at a faster rate than the top. The maximum temperature difference between the top and bottom of the tank reaches 4˚C, 24 h after the start of the experiment. This is because of the progressive development of thermal stratification at the bottom formed by the downward flow of cold water along the tank wall.

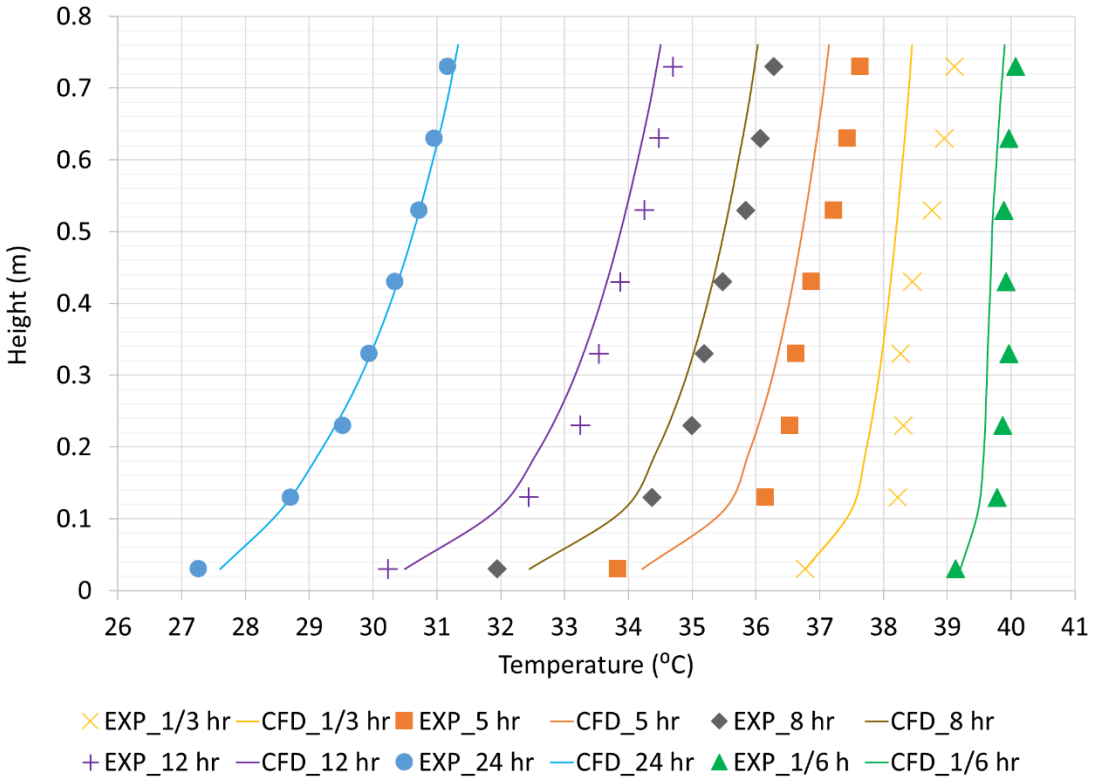

Figure 4. Temperature validation of CFD model for cool-down test

From these results, it is apparent that the temperature profile predicted by the CFD model is like that of the experiment. The same temperature trend can be observed between the two data sets (experiment and CFD) after 1/3 h (80 min) to 12 h of cooling, with deviations between the CFD prediction and the experimental data becoming negligible 24 h after the start of the cool-down test. The minor differences are likely due to the thermal stratification of the surrounding air during the experiment. As a result of heat loss from the tank, temperature of the air near the top of the tank could get higher than the one at the bottom of the tank. This possible variation of ambient temperature with height of the tank is not considered in the CFD model since the same ambient temperature has been specified at every section of the tank. The same behaviour was observed by Fan and Furbo (2012).

4.2. Velocity profile

Having shown that the thermal behavior of the storage tank could be characterized, it was necessary to determine if the hydrodynamic behavior could be too. In saying this, it is important to note that PIV images for three measurement planes could not be taken at the same time due to the transient nature of the problem. As such, two-dimensional velocity fields for the three measurement planes, at different times during the static cooling test, were captured along with a corresponding CFD prediction.

Figure 5 shows the time-averaged velocity contours at plane 3 for both the PIV and CFD between 80-82 min of the cooling test. From this the CFD model prediction compares reasonably well with the PIV data, displaying the initial formation of the hydrodynamic boundary layer near the wall due to heat losses from both top and side tank walls. A comparison of the PIV and CFD boundary layer velocity magnitude at a height of 1.18 m is shown in Figure 5 (c).

From these results it is apparent that the boundary layer thickness and velocity in the experiment were slightly larger than those predicted by the CFD model. The maximum velocity inside the boundary layer peaks at approximately 1.9 mm/s for the CFD, whereas the PIV peaks at 2.2 mm/s. This may be due to higher buoyancy forces in the experiment with respect to the CFD model as a result of higher tank temperature at the top as indicated in Figure 4. However, in general there is good agreement between the two results.

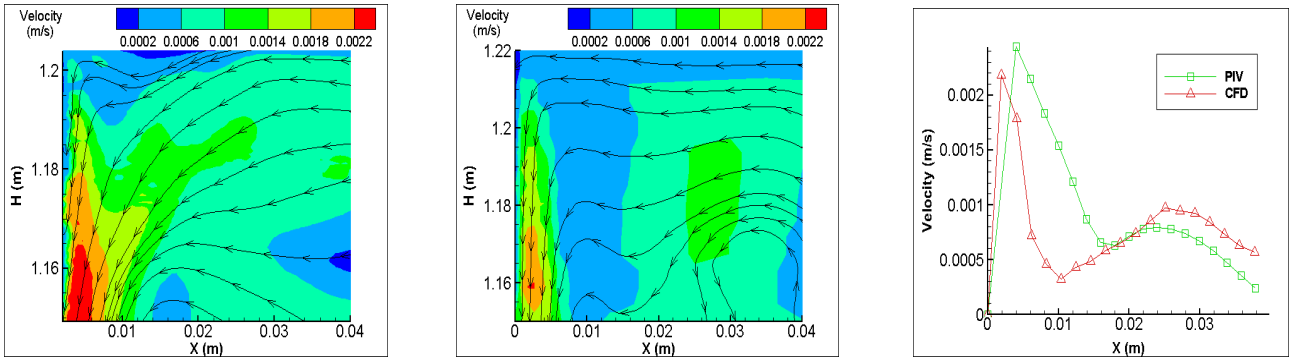

(a) (b) (c)

Figure 5. (a) Velocity field from experiment (left), and **(b)** CFD model (middle) at measurement plane 3 after 80 min of cooling, **(c)** Velocity magnitude along X = 0-37 mm at H = 1160 mm

Exploring the flow further, time-averaged flow patterns for plane 2 between 30-32 min of the cooling test are presented in Figure 6. Again, the CFD model agrees well with the experimental results. In these, it is apparent that there is a downward flow of cold water in the boundary layer and an upward flow of hot water far from the sidewall. The flow velocities in the boundary layer at 360 mm are plotted in Figure 6 (c) and again lower velocity values are estimated by CFD model, the highest velocity of 2.8 mm/s is seen in the numerical model, whereas PIV results showed the maximum velocity of 3.4 mm/s though they still correspond well with the experimental results. Again, this may be due to lower buoyancy forces in the CFD model because of the lower temperature at the tank top compared to the experiment.

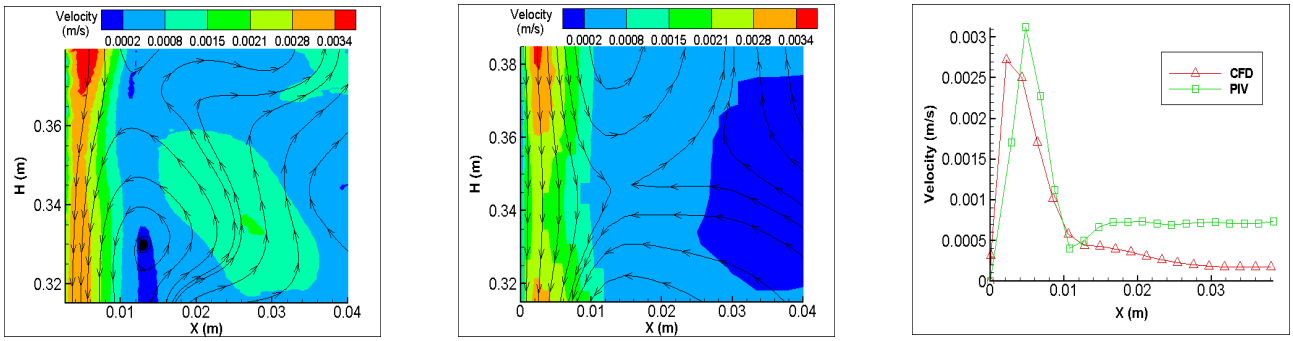

(a) (b) (c)

Figure 6. (a) Velocity field from experiment (left), and **(b)** CFD model (middle) at measurement plane 2 after 30 min of cooling, **(c)** Velocity magnitude along X = 0-37 mm at H = 360 mm

Finally, the velocity contours for plane 1 between 10-12 min of the cooling test are shown in Figure 7. Good validation of the numerical model is observed, with both displaying the detachment of the boundary layer, and flow into the center of the tank. The plot of velocities across the boundary layer at 80 mm indicate a velocity of approximately 2.2 mm/s in the PIV results, while the CFD model showed an estimate of 3.5 mm/s. This might be due to low level of thermal stratification in CFD model as a result of higher tank temperature at the bottom predicted by CFD model as opposed to the experiment.

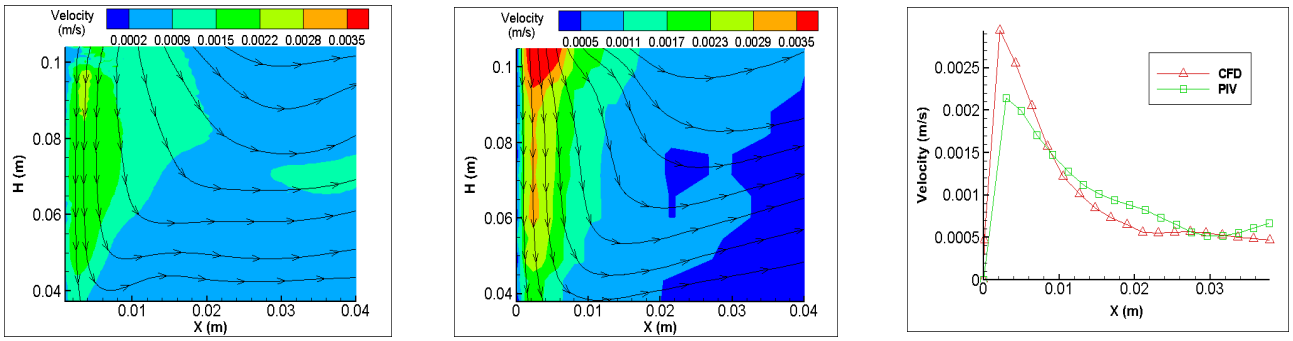

(a) (b) (c)

Figure 7. (a) Velocity field from experiment, and **(b)** CFD model at measurement plane 1 after 10 min of cooling, **(c)** Velocity magnitudes along X = 0-37 mm at H = 80 mm

Having shown that the CFD model was able to predict the flow and temperature fields, it was decided to explore the flow characteristics in greater detail. Hence the velocity contours at three different planes, after 10 min of cooling, were extracted as shown in Figure 8.

Due to the heat loss from the top wall, water is cooled and moves from the center of the tank the outside wall, instead of sinking directly down, because of the upward buoyancy force provided by the existing hot water underneath it. At the same time, hot water close to the side wall is cooled and travels downwards with a low peak velocity of 3.1 mm/s. When it combines with cold water that is flowing downwards in the middle, the velocity of the flow increases. Once it reaches the bottom of the tank, the velocity reduces again to about 3.1 mm/s due to the thermal stratification. This hinders the buoyancy driven boundary layer flow from travelling further and forces it to mix with the stratified layer of cold water at the bottom. Meanwhile, water in the center of the tank, close to the boundary layer, moves upwards at a relatively low

velocity compared to the boundary layer flow. More specifically, the buoyancy driven circulation leads to the formation of the velocity boundary layer which grows from 4 mm thickness at the top, to 8 mm in the middle sections and thins to about 6 mm thickness at the bottom.

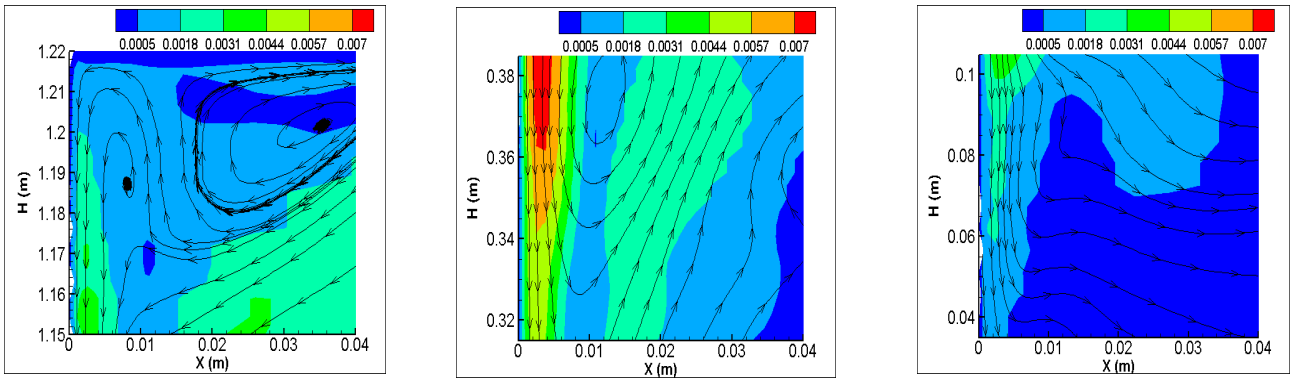

(a) (b) (c)

Figure 8. Velocity contours from CFD model after 10 min of cooling at **(a)** Plane 3, **(b)** Plane 2, **(c)** Plane 1

Inspecting the velocity contours at the same locations after 80 min of cooling, flow patterns like those at 10 min are observed, as shown in Figure 9. However, the velocities in the boundary layer are slower, as the tank has cooled down and thermal stratification has been developed in the middle and at the bottom of the tank. The buoyancy driven boundary layer flow increases from a peak velocity of 2.1 mm/s at the top to 2.5 mm/s in the middle sections and reduced to about 1.3 mm/s at the bottom of the tank.

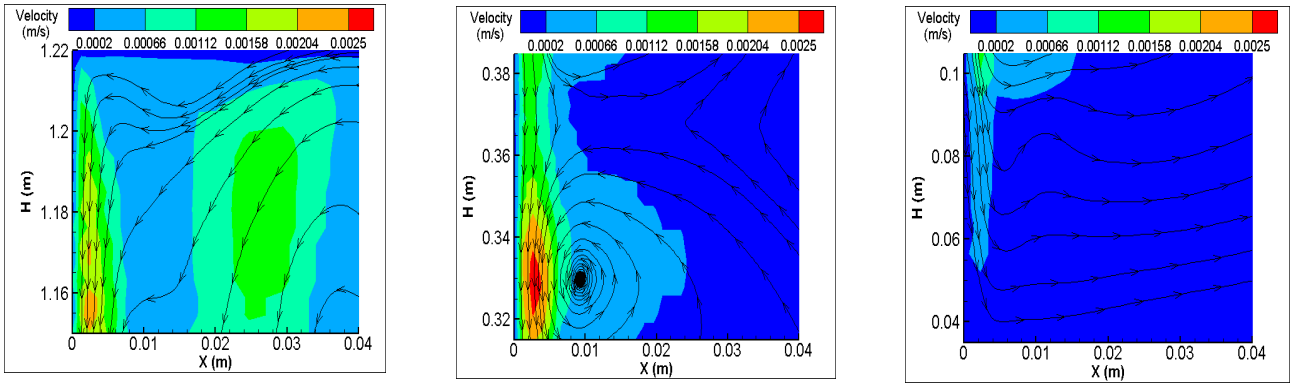

(a) (b) (c)

Figure 9. Velocity contours from CFD model after 80 min of cooling at (a) Plane 3, **(b)** Plane 2, **(c)** Plane 1

5. Conclusion

In conclusion, this work has characterised the natural convection in a rectangular storage tank under static cooling using PIV and a validated CFD model. The validated CFD model showed that the velocities are low at the top and bottom of the tank, in the order of 1-3 mm/s, while in the middle section velocities were over 3 mm/s. It was also found that the boundary layer grows in thickness in the middle section, while at the top and bottom, it is thinner. Hot water in the center of the tank was disturbed by the cooling at the top and side walls. Moreover, mixing of hot and cold water is seen at the top section while detachment of the boundary layer

flow at the bottom is observed. It is believed that the observed variations of boundary layer thickness and velocity along the height of the tank could be very useful in developing new measures to reduce heat loss to the surroundings and improve thermal performance of solar thermal hot water storage tanks.

References

Armstrong, P., Ager, D. Thompson, I. McCulloch, M. 2014. Improving the energy storage capability of hot water tanks through wall material specification. *Energy*, 78, p. 128-140.

Chandra, Y.P. and Matuska, T. 2019, "Stratification analysis of domestic hot water storage tanks: A comprehensive review"*, Energy and Buildings*, 187, p. 110-131.

Fan, J. and Furbo, S. 2012. Buoyancy driven flow in a hot water tank due to standby heat loss, *Solar Energy*, 86(11), p. 3438-3449.

Gasque, M., González-Altozano, P, Maurer, D, José Moncho-Esteve, I, Gutiérrez-Colomer, R.P., Palau-Salvador, G, and García-Marí, E., 2015, Study of the influence of inner lining material on thermal stratification in a hot water storage tank. *Applied Thermal Engineering*, 75: p. 344-356.

Jaluria, Y. and Gupta S.K., 1982. Decay of thermal stratification in a water body for solar energy storage. *Solar Energy*, 28(2): p. 137-143.

Kang, G.-U. and Chung, B.-J., 2010. The experimental study on transition criteria of natural convection inside a vertical pipe. *International Communications in Heat and Mass Transfer*, 37(8): p. 1057-1063.

Knudsen, S., Morrison, G.L., Behnia, M. and Furbo, S. 2005. Analysis of the flow structure and heat transfer in a vertical mantle heat exchanger. *Solar Energy*, 78(2): p. 281-289.

Mawire, A. and Taole, S., 2013. Heat loss estimation in a small vertical cylindrical stratified oil storage tank. *Proceedings of the 21st Domestic Use of Energy Conference Cape Town, South Africa,* 1-7

Miller, C. 1977. The effect of a conducting wall on a stratified fluid in a cylinder. in *12th Thermophysics Conference*.

Nelson, J.E.B., Balakrishnan, A.R. and Srinivasa Murthy S., 1999. Parametric studies on thermally stratified chilled water storage systems. *Applied Thermal Engineering*, 19(1): p. 89-115.

Oliveski, R.D.C., 2000. *Análise numérica e experimental dos campos de temperatura e velocidade em armazenadores térmicos.*

Roache, P., 1998, *Verification and Validation in Computational Science and Engineering.* Hermosa Publishers, Albuquerque, New Mexico, 1(99): p. 8.

Shah, L.J., Morrison, G.L., and Behnia, M. 1999. Characteristics of Vertical Mantle Heat Exchangers For Solar Water Heaters. *Solar Energy*, 67(1): p. 79-91.

Shyu, R.J. and Hsieh, C.K., 1987. Unsteady Natural Convection in Enclosures With Stratified Medium. *Journal of Solar Energy Engineering,* 109(2): p. 127-133.

Vliet, G.C. and Liu, C.K., 1969. An experimental study of turbulent natural convection boundary layers. *Journal of Heat Transfer*, 91(4): p. 517-531.

Yang, Z., Chen, H, Wang, L. Sheng,Y and Wang,Y, 2016. Comparative study of the influences of different water tank shapes on thermal energy storage capacity and thermal stratification. *Renewable Energy*, 85: p. 31-44.